Research Article | Vol. 25, No. 23 | 13 Nov 2017 | OPTICS EXPRESS 28684
Optics EXPRESS

Influence of microscopic and macroscopic effects on attosecond pulse generation using two-color laser fields

C. Chen,[1] C. Hernández-García,[2] Z. Tao,[1*] W. You,[1] Y. Zhang,[1] D. Zusin,[1] C. Gentry,[1] P. Tengdin,[1] A. Becker,[1] A. Jaron-Becker,[1] H. Kapteyn,[1] and M. Murnane[1]

[1]*Department of Physics and JILA, University of Colorado, Boulder, CO 80309-0440, USA*
[2]*Grupo de Investigación en Aplicaciones del Láser y Fotónica, Departamento de Física Aplicada, University of Salamanca, Salamanca 37008, Spain*
[*]*Zhensheng.Tao@jila.colorado.edu*

Abstract: Attosecond pulses and pulse trains generated by high-order harmonic generation are finding broad applications in advanced spectroscopies and imaging, enabling sub-femtosecond electron dynamics to be probed in atomic, molecular and material systems. To date, isolated attosecond pulses have been generated either by using very short few-cycle driving pulses, or by using temporal and polarization gating, or by taking advantage of phase-matching gating. Here we show that by driving high harmonics with a two-color linearly polarized laser field, the temporal window for time-gated phase matching is shorter than for the equivalent singe-color driving laser. As a result, we can generate quasi-isolated attosecond pulses with a peak width of ~ 450 as using relatively long 26 femtosecond laser pulses. Our experimental data are in good agreement with theoretical simulations, and show that the phase matching window decreases by a factor of 4 - from four optical cycles in the case of a single-color fundamental driving laser, to one optical cycle in the case of two-color (ω-2ω) laser drivers. Finally, we also demonstrate that by changing the relative delay between the two-color laser fields, we can control the duration of the attosecond bursts from 450 as to 1.2 fs.

OCIS codes: (190.4180) Multiphoton processes; (190.2620) Harmonic generation and mixing; (340.0340) X-ray optics; (300.6500) Spectroscopy, time-resolved.

References and links

1. A. Rundquist, C. G. Durfee III, Z. Chang, C. Herne, S. Backus, M. Murnane, and H. C. Kapteyn, "Phase-matched generation of coherent soft X-rays," Science **280**, 1412–1415 (1998).
2. J. L. Krause, K. J. Schafer, and K. C. Kulander, "High-order harmonic generation from atoms and ions in the high intensity regime," Phys. Rev. Lett. **68**, 3535–3538 (1992).
3. R. A. Bartels, A. Paul, H. Green, H. C. Kapteyn, M. Margaret, S. Backus, I. P. Christov, Y. Liu, D. Attwood, R. A. Bartels, A. Paul, H. Green, H. C. Kapteyn, M. M. Murnane, S. Backus, I. P. Christov, Y. Liu, D. Attwood, and C. Jacobsen, "Generation of spatially coherent light at extreme ultraviolet wavelengths," Science **297**, 376–378 (2002).
4. H. C. Kapteyn, M. M. Murnane, and I. P. Christov, "Extreme nonlinear optics: coherent X-Rays from lasers," Phys. Today **58**, 39 (2005).
5. A. Mcpherson, G. Gibson, H. Jara, U. Johann, T. S. Luk, I. A. Mcintyre, K. Boyer, and C. K. Rhodes, "Studies of multiphoton production of vacuum-ultraviolet radiation in the rare gases," J. Opt. Soc. Am. B **4**, 595–601 (1987).
6. T. Popmintchev, M. Chen, D. Popmintchev, P. Arpin, S. Brown, S. Ali, G. Andriukaitis, T. Bal, O. D. Mücke, A. Pugzlys, A. Baltu, B. Shim, S. E. Schrauth, A. Gaeta, C. Hernández-garcía, L. Plaja, A. Becker, A. Jaron-becker, M. M. Murnane, and H. C. Kapteyn, "Bright coherent ultrahigh harmonics in the keV X-ray regime from mid-Infrared femtosecond lasers," Science **336**, 1287–1291 (2012).
7. D. Popmintchev, C. Hernández-García, F. Dollar, C. Mancuso, J. A. Pérez-Hernández, M.-C. Chen, A. Hankla, X. Gao, B. Shim, A. L. Gaeta, M. Tarazkar, D. A. Romanov, R. J. Levis, J. A. Gaffney, M. Foord, S. B. Libby, A. Jaron-Becker, A. Becker, L. Plaja, M. M. Murnane, H. C. Kapteyn, and T. Popmintchev, "Ultraviolet surprise: Efficient soft x-ray high-harmonic generation in multiply ionized plasmas," Science **350**, 1225–1231 (2015).
8. M. Ferray, A. L'Huillier, X. F. Li, L. A. Lompré, G. Mainfray, and C. Manus, "Multiple-harmonic conversion of 1064 nm radiation in rare gases," J. Phys. B At. Mol. Opt. Phys. **21**, L31–L35 (1988).
9. X. Zhou, P. Ranitovic, C. W. Hogle, J. H. D. Eland, H. C. Kapteyn, and M. M. Murnane, "Probing and controlling non-Born-Oppenheimer dynamics in highly excited molecular ions," Nat. Phys. **8**, 232–237 (2012).

#296502 https://doi.org/10.1364/OE.25.028684
Journal © 2017 Received 3 Jul 2017; revised 20 Oct 2017; accepted 25 Oct 2017; published 3 Nov 2017

Optics EXPRESS

10. Y. Pertot, C. Schmidt, M. Matthews, A. Chauvet, M. Huppert, V. Svoboda, A. von Conta, A. Tehlar, D. Baykusheva, J. Wolf, and H. J. Wörner, "Time-resolved x-ray absorption spectroscopy with a water window high-harmonic source," Science **355**, 264–267 (2017).
11. S. Eich, A. Stange, A. V. Carr, J. Urbancic, T. Popmintchev, M. Wiesenmayer, K. Jansen, A. Ruffing, S. Jakobs, T. Rohwer, S. Hellmann, C. Chen, P. Matyba, L. Kipp, K. Rossnagel, M. Bauer, M. M. Murnane, H. C. Kapteyn, S. Mathias, and M. Aeschlimann, "Time- and angle-resolved photoemission spectroscopy with optimized high-harmonic pulses using frequency-doubled Ti:Sapphire lasers," J. Electron Spectrosc. Relat. Phenom. **195**, 231–236 (2014).
12. V. Gruson, L. Barreau, Á. Jiménez-Galan, F. Risoud, J. Caillat, A. Maquet, B. Carré, F. Lepetit, J.-F. Herǵott, T. Ruchon, L. Argenti, R. Taïeb, F. Martín, and P. Salières, "Attosecond dynamics through a Fano resonance: Monitoring the birth of a photoelectron," Science **354**, 734–738 (2016).
13. S. Hellmann, T. Rohwer, M. Kalläne, K. Hanff, C. Sohrt, A. Stange, A. Carr, M. M. Murnane, H. C. Kapteyn, L. Kipp, M. Bauer, and K. Rossnagel, "Time-domain classification of charge-density-wave insulators," Nat. Commun. **3**, 1069 (2012).
14. M. Kotur, D. Guénot, Á. Jiménez-Galán, D. Kroon, E. W. Larsen, M. Louisy, M. Bengtsson, M. Miranda, J. Mauritsson, C. L. Arnold, S. E. Canton, M. Gisselbrecht, T. Carette, M. J. Dahlström, E. Lindroth, A. Maquet, L. Argenti, F. Martín, and A. L'Huillier, "Spectral phase measurement of a Fano resonance using tunable attosecond pulses," Nat. Commun. **7**, 10566 (2016).
15. A. L. Cavalieri, N. Müller, T. Uphues, V. S. Yakovlev, A. Baltuška, B. Horvath, B. Schmidt, L. Blümel, R. Holzwarth, S. Hendel, M. Drescher, U. Kleineberg, P. M. Echenique, R. Kienberger, F. Krausz, and U. Heinzmann, "Attosecond spectroscopy in condensed matter," Nature **449**, 1029–1032 (2007).
16. M. Ossianer, F. Siegrist, V. Shirvanyan, R. Pazourek, A. Sommer, T. Latka, A. Guggenmos, S. Nagele, J. Feist, J. Burgdörfer, R. Kienberger, and M. Schultze, "Attosecond correlation dynamics," Nature Physics **13**, 280-285 (2017).
17. R. Locher, L. Castiglioni, M. Lucchini, M. Greif, L. Gallmann, J. Osterwalder, M. Hengsberger, and U. Keller, "Energy-dependent photoemission delays from noble metal surfaces by attosecond interferometry," Optica **2**, 405–410 (2015).
18. M. Reduzzi, P. Carpeggiani, S. Kühnc, F. Calegari, M. Nisoli, S. Stagira, C. Vozzi, P. Dombi, S. Kahaly, P. Tzallas, D. Charalambidis, K. Varju, K. Osvay, and G. Sansone, "Advances in high-order harmonic generation sources for time-resolved investigations," J. Electron Spectrosc. Relat. Phenom. **204**, 257–268 (2015).
19. J. Miao, T. Ishikawa, I. K. Robinson, and M. M. Murnane, "Beyond crystallography: Diffractive imaging using coherent x-ray light sources," Science **348**, 530–535 (2015).
20. D. Gardner, M. Tanksalvala, E. Shanblatt, X. Zhang, B. Galloway, C. Porter, R. Karl, C. Bevis, D. Adams, H. Kapteyn, M. Murnane, and G. Mancini, "Sub-wavelength coherent imaging of periodic samples using a 13.5nm tabletop high harmonic light source," Nat. Photonics **11**, 259–263 (2017).
21. C. Chen, Z. Tao, A. Carr, P. Matyba, T. Szilvási, S. Emmerich, M. Piecuch, M. Keller, D. Zusin, S. Eich, M. Rollinger, W. You, S. Mathias, U. Thumm, M. Mavrikakis, M. Aeschlimann, P. M. Oppeneer, H. Kapteyn, and M. Murnane, "Distinguishing attosecond electron-electron scattering and screening in transition metals," Proceedings of the National Academy of Science **114**, E5300–E5307 (2017).
22. Z. Tao, C. Chen, T. Szilvási, M. Keller, M. Mavrikakis, H. Kapteyn, and M. Murnane, "Direct time-domain observation of attosecond final-state lifetimes in photoemission from solids," Science **353**, 62–67 (2016).
23. K. J. Schafer, B. Yang, L. F. Dimauro, and K. C. Kulander, "Above threshold ionization beyond the high harmonic cutoff," Phys. Rev. Lett. **70**, 1599–1602 (1993).
24. P. B. Corkum, "Plasma perspective on strong-field multiphoton ionization," Phys. Rev. Lett. **71**, 1994–1997 (1993).
25. I. Christov, M. Murnane, and H. Kapteyn, "High-harmonic generation of attosecond pulses in the 'single-cycle' regime," Phys. Rev. Lett. **78**, 1251–1254 (1997).
26. P. B. Corkum, N. H. Burnett, and M. Y. Ivanov, "Subfemtosecond pulses," Opt. Lett. **19**, 1870–1872 (1994).
27. S. Gilbertson, Y. Wu, S. D. Khan, M. Chini, K. Zhao, X. Feng, and Z. Chang, "Isolated attosecond pulse generation using multicycle pulses directly from a laser amplifier," Phys. Rev. A **81**, 43810 (2010).
28. H. Mashiko, S. Gilbertson, C. Li, S. D. Khan, M. M. Shakya, E. Moon, and Z. Chang, "Double optical gating of high-order harmonic generation with carrier-envelope phase stabilized lasers," Phys. Rev. Lett. **100**, 130906 (2008).
29. G. Sansone, E. Benedetti, F. Calegari, C. Vozzi, L. Avaldi, R. Flammini, L. Poletto, P. Villoresi, C. Altucci, R. Velotta, S. Stagira, S. De Silvestri, and M. Nisoli, "Isolated Single-Cycle Attosecond Pulses," Science **314**, 443–446 (2006).
30. I. J. Sola, E. Mével, L. Elouga, E. Constant, V. Strelkov, L. Poletto, P. Villoresi, E. Benedetti, J.-P. Caumes, S. Stagira, C. Vozzi, G. Sansone, and M. Nisoli, "Controlling attosecond electron dynamics by phase-stabilized polarization gating," Nat. Phys. **2**, 319–322 (2006).
31. P. Tzallas, E. Skantzakis, C. Kalpouzos, E. P. Benis, G. D. Tsakiris, and D. Charalambidis, "Generation of intense continuum extreme-ultraviolet radiation by many-cycle laser fields," Nat. Phys. **3**, 846–850 (2007).
32. C. Hernández-García, T. Popmintchev, M. M. Murnane, H. C. Kapteyn, L. Plaja, A. Becker, and A. Jaron-Becker, "Isolated broadband attosecond pulse generation with near- and mid-infrared driver pulses via time-gated phase matching," Opt. Express **10**, 11855–11866 (2017).
33. M.-C. Chen, C. Mancuso, C. Hernández-García, F. Dollar, B.Fig. 2a Galloway, D. Popmintchev, P.-C. Huang, B. Walker, L. Plaja, A. A. Jaroń-Becker, A. Becker, M. M. Murnane, H. C. Kapteyn, and T. Popmintchev, "Generation of bright isolated attosecond soft X-ray pulses driven by multicycle midinfrared lasers," Proc. Natl. Acad. Sci. U. S. A. **111**, E2361–E2367 (2014).

Optics EXPRESS

34. T. Popmintchev, M.-C. Chen, A. Bahabad, M. Gerrity, P. Sidorenko, O. Cohen, I. P. Christov, M. M. Murnane, and H. C. Kapteyn, "Phase matching of high harmonic generation in the soft and hard X-ray regions of the spectrum," Proc. Natl. Acad. Sci. U. S. A. **106**, 10516–10521 (2009).
35. I. Thomann, A. Bahabad, X. Liu, R. Trebino, M. M. Murnane, and H. C. Kapteyn, "Characterizing isolated attosecond pulses from hollow-core waveguides using multi-cycle driving pulses," Opt. Express **17**, 4611–4633 (2009).
36. S. Watanabe, K. Kondo, Y. Nabekawa, A. Sagisaka, and Y. Kobayashi, "Two-color phase control in tunneling ionization and harmonic generation by a strong laser field and its third harmonic," Phys. Rev. Lett. **73**, 2692–2695 (1994).
37. J. Mauritsson, P. Johnsson, E. Gustafsson, A. L'Huillier, K. J. Schafer, and M. B. Gaarde, "Attosecond pulse trains generated using two color laser fields," Phys. Rev. Lett. **97**, 13001 (2006).
38. M. D. Perry and J. K. Crane, "High-order harmonic emission from mixed fields," Phys. Rev. A **48**, R4051–R4054 (1993).
39. U. Andiel, G. D. Tsakiris, E. Cormier, and K. Witte, "High-order harmonic amplitude modulation in two-colour phase-controlled frequency mixing," Europhys. Lett. **47**, 42–48 (1999).
40. I. J. Kim, C. M. Kim, H. T. Kim, G. H. Lee, Y. S. Lee, J. Y. Park, D. J. Cho, and C. H. Nam, "Highly efficient high-harmonic generation in an orthogonally polarized two-color laser field," Phys. Rev. Lett. **94**, 243901 (2005).
41. D. Charalambidis, P. Tzallas, E. P. Benis, E. Skantzakis, G. Maravelias, L. A. A. Nikolopoulos, A. P. Conde, and G. D. Tsakiris, "Exploring intense attosecond pulses," N. J. Phys. **10**, 025018 (2008).
42. C. Chen, Z. Tao, C. Hernández-García, P. Matyba, A. Carr, R. Knut, O. Kfir, D. Zusin, C. Gentry, P. Grychtol, O. Cohen, L. Plaja, A. Becker, A. Jaron-Becker, H. Kapteyn, and M. Murnane, "Tomographic reconstruction of circularly polarized high-harmonic fields: 3D attosecond metrology," Sci. Adv. **2**, e1501333 (2016).
43. S. Long, W. Becker, and J. K. McIver, "Model calculations of polarization-dependent two-color high-harmonic generation," Phys. Rev. A **52**, 2262–2278 (1995).
44. O. Kfir, P. Grychtol, E. Turgut, R. Knut, D. Zusin, D. Popmintchev, T. Popmintchev, H. Nembach, J. M. Shaw, A. Fleischer, H. Kapteyn, M. Murnane, and O. Cohen, "Generation of bright phase-matched circularly-polarized extreme ultraviolet high harmonics," Nat. Photonics **9**, 99–105 (2014).
45. G. Laurent, W. Cao, I. Ben-Itzhak, and C. L. Cocke, "Attosecond pulse characterization," Opt. Express **21**, 16914–16927 (2013).
46. G. Laurent, W. Cao, H. Li, Z. Wang, I. Ben-Itzhak, and C. L. Cocke,"Attosecond control of orbital parity mix interferences and the relative phase of even and odd harmonics in an attosecond pulse train," Phys. Rev. Lett. **109**, 083001 (2012).
47. R. López-Martens, K. Varjú, P. Johnsson, J. Mauritsson, Y. Mairesse, P. Salières, M. B. Gaarde, K. J. Schafer, A. Persson, S. Svanberg, C. G. Wahlström, and A. L'Huillier, "Amplitude and phase control of attosecond light pulses," Phys. Rev. Lett. **94**, 33001 (2005).
48. X. He, J. M. Dahlström, R. Rakowski, C. M. Heyl, A. Persson, J. Mauritsson, and A. L'Huillier, "Interference effects in two-color high-order harmonic generation," Phys. Rev. A **82**, 33410 (2010).
49. E. Goulielmakis, M. Schultze, M. Hofstetter, V. S. Yakovlev, J. Gagnon, M. Uiberacker, A. L. Aquila, E. M. Gullikson, D. T. Attwood, R. Kienberger, F. Krausz, and U. Kleineberg, "Single-Cycle Nonlinear Optics," Science **320**, 1614–1617 (2008).
50. E. J. Takahashi, P. Lan, O. D. Mücke, Y. Nabekawa, and K. Midorikawa, "Infrared two-color multicycle laser field synthesis for generating an intense attosecond pulse," Phys. Rev. Lett. **104**, 233901 (2010).
51. W. Holgado, C. Hernández-García, B. Alonso, M. Miranda, F. Silva, L. Plaja, H. Crespo, and I. J. Sola, "Continuous spectra in high-harmonic generation driven by multicycle laser pulses," Phys. Rev. A **93**, 13816 (2016).
52. M. Chini, S. Gilbertson, S. D. Khan, and Z. Chang, "Characterizing ultrabroadband attosecond lasers," Opt. Express **18**, 13006–13016 (2010).
53. C. Hernández-García, J. A. Pérez-Hernández, J. Ramos, E. C. Jarque, L. Roso, and L. Plaja, "High-order harmonic propagation in gases within the discrete dipole approximation," Phys. Rev. A **82**, 33432 (2010).
54. C. Hernández-García, T. Popmintchev, M. M. Murnane, H. C. Kapteyn, L. Plaja, A. Becker, and A. Jaron-Becker, "Group velocity matching in high-order harmonic generation driven by mid-infrared lasers," New J. Phys. **18**, 73031 (2016).
55. M. V. Ammosov, N. B. Delone, and V. P. Kraĭnov, "Tunnel ionization of complex atoms and of atomic ions in an alternating electromagnetic field," Sov. Phys. JETP **64**, 1191–1194 (1986).
56. C. G. Durfee III, A. R. Rundquist, S. Backus, C. Herne, M. Murnane, and H. Kapteyn, "Phase matching of high-order harmonics in hollow waveguides," Phys. Rev. Lett. **83**, 2187–2190 (1999).
57. S. Kazamias, D. Douillet, F. Weihe, C. Valentin, A. Rousse, S. Sebban, G. Grillon, F. Augé, D. Hulin, and Ph. Balcou, "Global optimization of high harmonic generation," Phys. Rev. Lett. **90**, 193901 (2003).
58. D. D. Hickstein, F. J. Dollar, P. Grychtol, J. L. Ellis, R. Knut, C. Hernández-García, D. Zusin, C. Gentry, J. M. Shaw, T. Fan, K. M. Dorney, A. Becker, A. Jaroń-Becker, H. C. Kapteyn, M. M. Murnane, and C. G. Durfee,"Non-collinear generation of angularly isolated circularly polarized high harmonics," Nat. Photonics **9**, 743–750 (2015).
59. J. B. Bertrand, H. J. Wörner, H. C. Bandulet, É. Bisson, M. Spanner, J.-C. Kieffer, D. M. Villeneuve, and P. B. Corkum, "Ultrahigh-order wave mixing in noncollinear high harmonic generation," Phys. Rev. Lett. **106**, 023001 (2011).
60. L. Rego, J. S. Román, A. Picón, L. Plaja, and C. Hernández-García, "Nonperturbative twist in the generation of

Optics EXPRESS

extreme-ultraviolet vortex beams," Phys. Rev. Lett. **117**, 163202 (2016).
61. E. Constant, D. Garzella, P. Breger, E. Mével, C. Dorrer, C. Le Blanc, F. Salin, and P. Agostini, "Optimizing high harmonic generation in absorbing gases: model and experiment," Phys. Rev. Lett. **82**, 1668–1671 (1999).
62. Y. Tamaki, J. Itatani, Y. Nagata, M. Obara, and K. Midorikawa, "Highly efficient, phase-matched high-harmonic generation by a self-guided laser beam," Phys. Rev. Lett. **82**, 1422–1425 (1999).
63. B. L. Henke, E. M. Gullikson, and J. C. Davis, "X-Ray interactions: photoabsorption, scattering, transmission, and reflection at E = 50-30,000 eV, Z = 1-92," At. Data Nucl. Data Tables **54**, 181–342 (1993).
64. J. Tate, T. Auguste, H. G. Muller, P. Salières, P. Agostini, and L. F. DiMauro, "Scaling of wave-packet dynamics in an intense midinfrared field," Phys. Rev. Lett. **98**, 013901 (2007).
65. J. A. Pérez-Hernández, L. Roso, and L. Plaja, "Harmonic generation beyond the strong-field approximation: the physics behind the short-wave-infrared scaling laws," Opt. Express **12**, 9891–9903 (2009).
66. P. Antoine, B. Piraux, and A. Maquet, "Time profile of harmonics generated by a single atom in a strong electromagnetic field," Phys. Rev. A **51**, R1750–R1753 (1995).

1. Introduction

Coherent laser-like beams spanning the extreme ultraviolet (EUV) and soft X-ray spectral regions can be generated via high-order harmonic upconversion of an intense driving laser field in a gas medium [1–8]. The exquisite spatial and temporal coherence of high harmonic generation (HHG) produces attosecond pulses and pulse trains that are perfectly synchronized to the driving laser, with ultrastable coherent wavefronts, all in a tabletop-scale setup. As a result, applications of HHG for probing matter at the spatio-temporal limits relevant to function are rapidly increasing. In exciting recent work, HHG sources were used to capture chemical reactions in real time [9, 10], to reveal correlated charge, spin and phonon dynamics in materials with femtosecond-to-attosecond time resolution [11–18], and to demonstrate the first sub-wavelength EUV/X-ray imaging of nanostructures [19, 20]. In particular, a new technique called attosecond-ARPES (angle resolved photoemission) harnesses HHG pulse trains to measure the fastest electron dynamics intrinsic to materials, making it possible to distinguish sub-femtosecond electron scattering and screening for the first time [21, 22]. The temporal structure of HHG pulse trains is determined by the electron wavepacket dynamics driven by a strong laser field. In the semi-classical picture, when an atom is irradiated by an intense ultrafast laser pulse, the electron first tunnels through the Coulomb barrier and is then accelerated away from its parent ion. When the laser field reverses direction and drives the electron back to recollide with its parent ion, a HHG photon is emitted in the recombination step [23, 24]. When driven by a single-color linearly-polarized laser field, this process repeats twice every cycle of the laser field. Therefore, one approach for generating isolated attosecond pulses is to reduce the number of laser-field cycles, in order to confine the recombination events to the most intense half cycle of the driving field [25]. However, this only considered HHG from a single atom, which emerges as weak dipole radiation. More advanced approaches take phase matching into account - that is needed in order to generate either a HHG beam or make it bright for applications. These include phase-matching gating or polarization gating techniques that restrict the HHG process to one single half cycle of the driving field. Temporal polarization gating takes advantage of the dependence of the HHG efficiency on the circularity of the driving fields by superposing various combinations of circularly and linearly polarized fields to create a short temporal window when the driving laser field is linearly polarized [26–31]. In contrast, phase-matching gating harnesses the fact that bright HHG beams can only be emitted during a finite time window, when the laser and HHG fields travel at the same velocity in the gas, allowing the HHG emission from many atoms to add coherently. This window of phase matching naturally ranges from a single half-cycle of the laser field for mid-IR driving lasers, to multiple half-cycles, for blue and UV driving lasers [7, 32–35].

It has been long realized that the HHG emission can be controlled by introducing a second driving field with a different wavelength, which breaks the symmetry of the electron recollision dynamics [36–41]. Indeed, two-color driven HHG has been shown to be useful in manipulating the temporal profile and polarization state of the emitted attosecond pulses, as well as relaxing

Optics EXPRESS

the conditions for single attosecond pulse generation. For example, the double optical gating technique introduces a second-harmonic pulse with an orthogonal/rotating polarization to enable polarization gating, resulting in isolated attosecond pulses [28]. Recently, circularly polarized attosecond pulses have been generated and characterized by using bi-chromatic circularly polarized driving fields with opposite helicities to drive HHG [42–44]. Moreover, when the polarization of the two fields is the same, attosecond pulses are emitted once per IR optical cycle and hence are carrier-envelop phase stabilized [37]. We note that the temporal structure of attosecond pulse sequences generated by linearly-polarized two-color laser fields has been previously studied with the second-harmonic field strength <0.5% of the IR field, leading to attosecond pulses emitted twice per IR-light cycle [45, 46]. However, the macroscopic phase matching conditions under the two-color geometry were not explored in these studies. This deficiency is important to address because in the case of two-color linearly-polarized driving lasers, macroscopic phase matching effects could be used to sculpt the intensity, phase, spectrum and duration of the emitted HHG pulses, by tailoring the phase matching window [1, 33]. This would add to our capabilities for coherently engineering attosecond waveforms using the two-color driving fields.

In this paper, by using laser-assisted photoemission to measure the full HHG field, we extend the concept of phase-matching gating of high harmonic generation to two-color laser fields, and show that it is quite distinct from phase-matching gating in a one-color laser field. Quasi-isolated attosecond pulses, with a peak width of ~450 as, can be generated by mixing a multi-cycle 26 fs, 780 nm, laser field with its second harmonic. By comparing our measurements with the results of numerical simulations, we show that the temporal window for HHG phase matching in this two-color (ω-2ω) configuration is shorter than the case of a single-color driving laser - decreasing by a factor of 4, from four optical cycles (for a single-color fundamental driver) to one optical cycle (in the case of two-color laser drivers). We also demonstrate that the resulting attosecond waveforms can be easily modulated by changing the relative phase delay between the 390 nm and 780 nm driving fields (φ_{RB}). Our results show that at the phase delay corresponding to the maximum HHG yield, the FWHM (full width at half maximum) of the attosecond bursts reaches a minimum value of 450 as, which is close to the value expected for the transform-limited case. In contrast, as the phase delay is adjusted away from the optimum HHG yields, the pulse FWHM is significantly increased due to the emergence of additional temporal structures. By comparing our experimental data with the results of numerical simulations and semiclassical calculations of the driving-field structure and electron trajectories, we find this observation is a direct consequence of the broken symmetry introduced by the intense second-harmonic field, which strongly modifies the electron ionization, propagation and recombination dynamics during the HHG process.

2. Experimental and numerical methods

2.1. Experimental setup

Our experimental setup is illustrated in Fig. 1(a). A linearly polarized HHG beam is generated by mixing a near-infrared field (ω, 780 nm, IR) with its second-harmonic field (2ω, 390 nm, blue) in a Mach-Zehnder interferometer. The FWHM pulse duration of the IR pulse is 26 fs. The polarizations of the two driving fields are adjusted to be parallel to each other, before they are focused collinearly into a 10-mm-long waveguide filled with Argon gas at a pressure of 30 torr. As a result, the HHG beam inherits the polarization of the combined driving fields. In our experiments, the two-color driving fields can be described as $E(t) = E_R \sin(\omega t) + E_B \sin(2\omega t + \varphi_0 + \varphi_{RB})$, where E_R and E_B are the amplitudes of the infrared (R) and blue (B) driving fields, respectively. Here, φ_0 is the relative phase delay between the two laser fields corresponding to the highest HHG yields, while φ_{RB} can be adjusted using a delay stage stabilized to sub-fs precision, as shown in Fig. 1a. The ω and 2ω beams are focused using lenses of focal length 50 cm (ω) and 75 cm (2ω), respectively, before propagating into a 10-mm-long fiber waveguide. As a result, the

Optics EXPRESS

peak intensity of the IR driving field is 1.5×10^{14} W/cm^2. To enhance the symmetry breaking between neighboring cycles in HHG, we use a strong blue driving field in our experiments, with a field intensity approximately half that of the IR field ($I_{2\omega} \approx 0.7 \times 10^{14}$ W/cm^2).

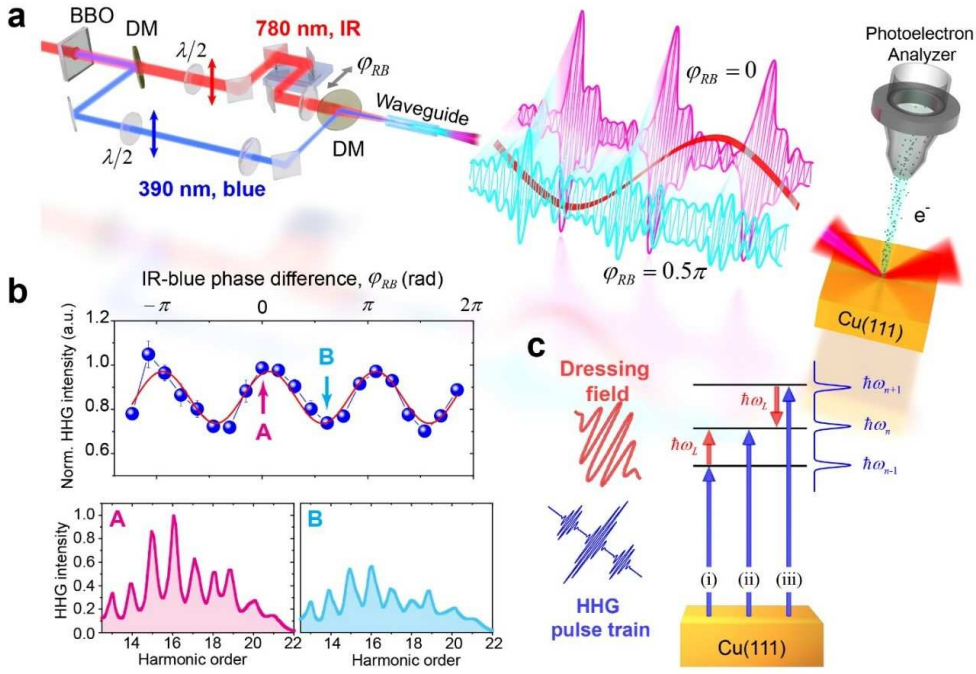

Fig. 1. Characterizing high-order harmonics generated using laser-assisted photoemission. a) Linearly polarized ω (780nm) and 2ω (390nm) beams from a Ti:Sapphire laser are focused into an Ar-filled hollow waveguide. The generated linearly polarized HHG and a time-delayed p-polarized 780nm dressing field are focused onto a clean Cu(111) surface. In experiments, the temporal structure of the attosecond bursts can be adjusted by the relative phase between the ω and 2ω driving fields, φ_{RB}. b) Upper panel: Modulation of the total HHG intensity as a function of φ_{RB}. Lower panel: The HHG spectra measured at the maximum (A) and the minimum (B) HHG intensities. The spectra were de-convoluted by considering the transmission rate of 200 nm Al filter [47]. c) Illustration of the quantum path interference of the interferometric laser-assisted photoemission with HHG field generated by ω-2ω driving fields.

The HHG spectra are measured directly using an EUV spectrometer with an energy resolution of ~100 meV, after travelling through a 200 nm Aluminum filter to block the residual driving laser fields. The spectra plotted in Fig. 1(b) are corrected by considering the transmission of the Al filter, as reported in [47]. As shown in Fig. 1(b), the spectra comprise of both odd and even orders of harmonics with comparable intensity, consistent with previous studies [37, 48]. By adjusting φ_{RB}, we can control the total HHG yield with high precision, showing a modulation of the total yield with a periodicity corresponding to half optical cycle of the blue laser field [37, 48] (Fig. 1(b)). This is a clear evidence that the harmonics are indeed generated by the two-color laser field. Notably, we observe a strong continuum background in our HHG spectra, suggesting that the harmonic radiation is emitted in the form of an quasi-isolated pulse [25, 29, 49, 50] - although quasi-continuum HHG radiation can also be emitted for appropriate phase relationships between several pulses [51]. We note that the continuum background is absent in spectra measured using the same spectrometer for the circularly polarized HHG driven by the circularly polarized two-color driving fields with similar field strength [42], indicating that this continuum background

Optics EXPRESS

is intrinsic to HHG emission.

To fully reconstruct the temporal structure of the HHG pulse train, we measure the spectral phases of the generated linearly polarized HHG beam by using attosecond metrology techniques [42, 52]. In this method, we focus the HHG beam onto a clean Cu(111) surface to induce photoemission. The photoelectrons are simultaneously modulated by a linearly polarized IR field, which propagates collinearly with the HHG beam. The IR dressing field is separated from the fundamental laser beam before second-harmonic generation, and hence only consists of the laser field at a wavelength of 780 nm ($\hbar\omega_L$=1.6 eV). The relative time delay between the HHG pulse and IR dressing pulse (τ_d) can be adjusted by a second delay stage in our experiments. Both the HHG and the IR dressing fields are adjusted to be p-polarized relative to the sample surface. Due to the existence of both even and odd harmonics, the photoelectron yield at the kinetic energy corresponding to the direct excitation by n^{th} order harmonics ($\hbar\omega_n$) is modulated due to the interference (Fig. 1(c)) between three quantum paths: (i) absorbing an HHG and an IR photon ($\hbar\omega_{n-1} + \hbar\omega_L$); (ii) direct photoemission by a single HHG photon ($\hbar\omega_n$); and (iii) absorbing an HHG photon and emitting an IR photon ($\hbar\omega_{n+1} - \hbar\omega_L$). The photoelectron yields as a function of τ_d are recorded using a hemispherical photoelectron analyzer, which gives rise to the interferograms shown in Fig. 2(a). Our method was recently successfully implemented to reconstruct circularly polarized HHG pulses [42].

2.2. Numerical simulations

In order to understand the HHG fields produced by the two-color (ω-2ω) driving laser fields, we performed numerical macroscopic HHG simulations by combining the strong-field approximation for the single atom response with discrete dipole approximation for the electromagnetic field propagator [53]. In this approach, the harmonics are assumed to propagate at the speed of light. However, for the driving laser fields, the dispersion of the neutral atoms, plasma and waveguide, as well as group-velocity mismatch [54], must be taken into account. Note that we also account for time-dependent ionization (computed via the ADK rates for the total electric field [55]), which gives rise to nonlinear phase shifts in the driving field (note that spatial nonlinearities are not included). In our simulations, the driving pulses are modelled as a $\sin^2$ envelope with the FWHM pulse duration of τ_R = 26 fs and τ_B = 35 fs for fields with wavelengths λ_R=775 nm (ω) and λ_B=387.5 nm (2ω), respectively. The peak intensities are 1.2×10^{14} W/cm^2 for the λ_R field, while the intensity of the λ_B field is half of that of the λ_R field, which were selected to be similar to the experimental conditions.

3. Quasi-isolated attosecond pulse

In Fig. 2(a), we plot the interferogram of photoelectrons excited by HHG beam at $\varphi_{RB} \approx 0$, which gives the highest HHG yield. The yields of the photoelectrons excited by different harmonic orders from the same d band of Cu(111) oscillate with a frequency of ω_L as a function of τ_d. In recent work, we have shown that the final-state resonance could affect the photoemission time delay from the low-energy d band with Λ_3 symmetry in transition metals. However, the resonant time delay only presents in a small range of the electron transverse momentum (electron emission angle within ± 3.5^o) and sharply decrease to a very small value (<50 as) at large angles [22]. In this work, we average the photoemission intensity across a large emission angle (± 13 ^{o}) in order to reduce the time delay induced by final-state resonance, as well as increase the signal-to-noise ratio in the analysis. At the same time, we note that the photoemission intensities of Λ_1 bands in copper are generally much higher than that of Λ_3 band and they contribute small photoemission time delay smooth across the energy range of measurements [22]. As a result, the time delay associated with the photoemission process itself is negligible in this work [42]. Information about the harmonic phases [$\phi(\omega_n)$] is encoded in the phases of the modulations in the interferogram [$\alpha(\omega_n)$], which is given by [42, 52]

Optics EXPRESS

$$\tan[\alpha(\omega_n)] = \frac{\sqrt{I_0(\omega_{n+1})}\sin[\phi(\omega_n) - \phi(\omega_{n+1})] - \sqrt{I_0(\omega_{n-1})}\sin[\phi(\omega_{n-1}) - \phi(\omega_n)]}{\sqrt{I_0(\omega_{n+1})}\cos[\phi(\omega_n) - \phi(\omega_{n+1})] - \sqrt{I_0(\omega_{n-1})}\cos[\phi(\omega_{n-1}) - \phi(\omega_n)]} \quad (1)$$

where $I_0(\omega_n)$ is the power spectrum. Using a genetic algorithm (details are described in [42]), we can retrieve the harmonic phases which best fit the measured interferogram phases. The fitting results are plotted in the right panel of Fig. 2(a), for $\varphi_{RB} \approx 0$. The measured HHG phases are plotted in Fig. 2(b) for both $\varphi_{RB} \approx 0$ and $\varphi_{RB} \approx 0.5\pi$. We find that the HHG phases as a function of harmonic order gradually evolve from the original linear shape to an "S" shape, as φ_{RB} changes from 0 to 0.5π. This trend can be successfully reproduced by the theoretical single-atom response, as shown in the inset of Fig. 2(b).

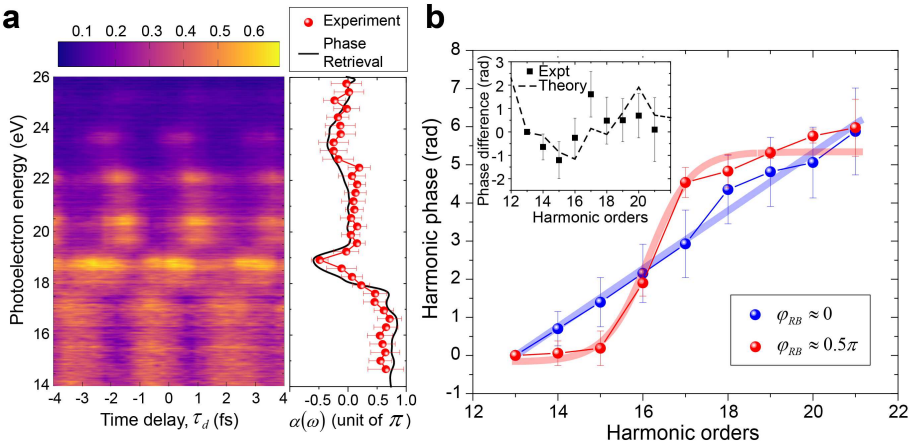

Fig. 2. Measuring the harmonic phases. a) 2D map of photoelectron yields at $\varphi_{RB} \approx 0$ as a function of photoelectron energy and pump-probe time delay (τ_d). The experimentally measured interferogram phase $\alpha(\omega)$ as a function of photoelectron energy is plotted in the right panel, in comparison with the reconstructed phases obtained from phase retrieval program (black solid line). The good agreement between the two indicates that the correct harmonic phases are retrieved from the experimental results. b) Phases of major harmonic orders measured at $\varphi_{RB} \approx 0$ and $\varphi_{RB} \approx 0.5\pi$. The uncertainty is determined as the standard deviation of phase values retrieved from multiple trials. For the comparison, the harmonic phases for both cases are offset so that the phase of the 13th harmonic is zero. The solid lines highlight the variation of the harmonic phases and serve the purpose of guiding the eyes. The difference of harmonic phases between $\varphi_{RB} \approx 0.5\pi$ and $\varphi_{RB} \approx 0$ is plotted in the inset. The phase difference obtained in our numerical simulation is also plotted for comparison (dashed line).

With the HHG spectral intensities and phases measured, the time-domain structure of the HHG field can therefore be reconstructed. The temporal profile of HHG pulse train corresponding to $\varphi_{RB} \approx 0$ is plotted in Fig. 3(a). The profile is observed to be a quasi-isolated attosecond pulse with a pulse width of ~ 450 as (FWHM), accompanied by two attosecond bursts with amplitude weaker by a factor of 5, separated from the center pulse by one optical cycle of the fundamental IR field. The pulse width is very close to the transform-limited value (dashed line in Fig. 3(a)), which is consistent with the linear dependence of HHG phases as a function of harmonic order, as shown in Fig. 2(b). When φ_{RB} is changed to 0.5π, we observe additional attosecond bursts in the temporal domain (Fig. 3(b)).

Optics EXPRESS

Obviously, the generation of quasi-isolated attosecond pulses driven by multicycle laser fields cannot be explained by a single-atom response of the HHG process. In order to understand these results, we must consider the macroscopic response of the medium by extending the time-gated phase matching concept [32–35, 56] to a two-color driving laser field. In a hollow waveguide, the phase mismatch of the q^{th} order harmonic ($\Delta k_q^{\omega-2\omega}$) can be estimated by considering the net dispersion due to the waveguide, the free-electron plasma as well as the neutral atoms. In the presence of a second harmonic driver (λ_B), this becomes

$$\begin{aligned}\Delta k_q^{\omega-2\omega}(t) \approx & \Delta k_q^{\text{waveguide}} + \Delta k_q^{\text{plasma}} + \Delta k_q^{\text{neutral}} \\ \approx & \{n_R \frac{\lambda_R u_{11}^2}{4\pi a^2} + 2n_B \frac{\lambda_B u_{11}^2}{4\pi a^2}\} + \{n_R P \frac{\lambda_R e^2}{m_e c^2}\eta(t) + 2n_B P \frac{\lambda_B e^2}{m_e c^2}\eta(t)\} \\ & -\{n_R P \frac{4\pi^2 \chi_0}{\lambda_R}[1-\eta(t)] + 2n_B P \frac{4\pi^2 \chi_0}{\lambda_B}[1-\eta(t)]\}\end{aligned} \tag{2}$$

where $\eta(n)$ is the time-dependent ionization rate, χ_0 is the linear susceptibility of the gas due to the neutrals and P is the gas pressure inside the waveguide. We note that in the harmonic generation process, $n_R(n_B)$ photons were absorbed from the λ_R (λ_B) field, so we have $q = n_R + 2n_B$. In Eq. (2), we have calculated the waveguide dispersion term, where a is the waveguide radius and $u_{11} = 2.405$ is the first zero of the Bessel function J_0 [33, 56]. One can also define the coherence length as $L_{\text{coh}}^{\omega-2\omega,q}(t) = \pi/\Delta k_q^{\omega-2\omega}(t)$, in a similar way as it was performed in [57] for the single-color geometry. Perfect phase matching occurs when the three terms in Eq. (2) are perfectly compensated ($\Delta k_q^{\omega-2\omega,q}(t) = 0$), which happens at a critical ionization level. This condition is achieved during a finite temporal window during which the harmonic signal builds up constructively, which determines the number of attosecond pulses that are efficiently emitted.

In Fig. 3(c), we compare the calculated time-dependent coherence length for one-color (λ_R=775 nm, dashed line) and two-color (λ_R=775 nm, λ_B=387.5 nm, solid lines) driving fields in a 30 torr Ar-filled waveguide (a=75 μm). The peak intensity of the one-color driving field is chosen to be 1.3×10^{14} W/cm^2. The peak intensities for the two-color configuration are the same as those used in the numerical simulations. In Fig. 3(c), we plot the time-dependent coherence length for the 21$^{\text{st}}$ harmonic ($L_{\text{coh}}^{\omega,H21}$, dashed black) in the one-color configuration, whereas for the two-color case we compare results for the 15$^{\text{th}}$ harmonic with n_R=n_B=5 ($L_{\text{coh}}^{\omega-2\omega,H15}$, solid red), the 18$^{\text{th}}$ harmonic with n_R=n_B=6 ($L_{\text{coh}}^{\omega-2\omega,H18}$, solid green) and the 21$^{\text{st}}$ harmonic with n_R=n_B=7 ($L_{\text{coh}}^{\omega-2\omega,H21}$, solid blue). Note that there are many different photon combinations, but for simplicity we have selected those where n_R=n_B. The appearance of different absorption channels in phase-matching would be similar to that occurring in non-collinear [58, 59] or vortex-combination [60] HHG schemes, but such an analysis lies beyond the scope of this paper. The optimal phase-matching conditions are achieved if $L_{\text{coh}} > 5L_{\text{abs}}$ (pink dot-dashed line) where L_{abs} is the absorption length [61]. One can clearly observe that introducing the second-harmonic driver significantly reduces the phase-matching window from ~ 4 optical cycles of the fundamental IR field in the one-color configuration, to less than 1 optical cycle in the two-color configuration, allowing for the generation of few attosecond bursts driven by multicycle laser fields. We also performed numerical macroscopic HHG simulations by considering different propagation lengths (L) in the gas-filled waveguide, the results of which are plotted in Fig. 3(d). Indeed, the harmonic emission is confined to few attosecond bursts as the medium length is increased to L=10 mm, in very good agreement with the analytical results presented in Fig. 3(c), and with our experimental observations. We note that the gas-filled hollow waveguide is critical for the generation of quasi-isolated attosecond pulses in this experiment, because it provides a sufficiently long laser-medium interaction length (10 mm in our case) to ensure strong temporal gating due to macroscopic phase matching. On the other hand, we believe similar temporal gating can also be achieved in a gas cell with sufficient pressure and interaction length [33, 62]

Optics EXPRESS

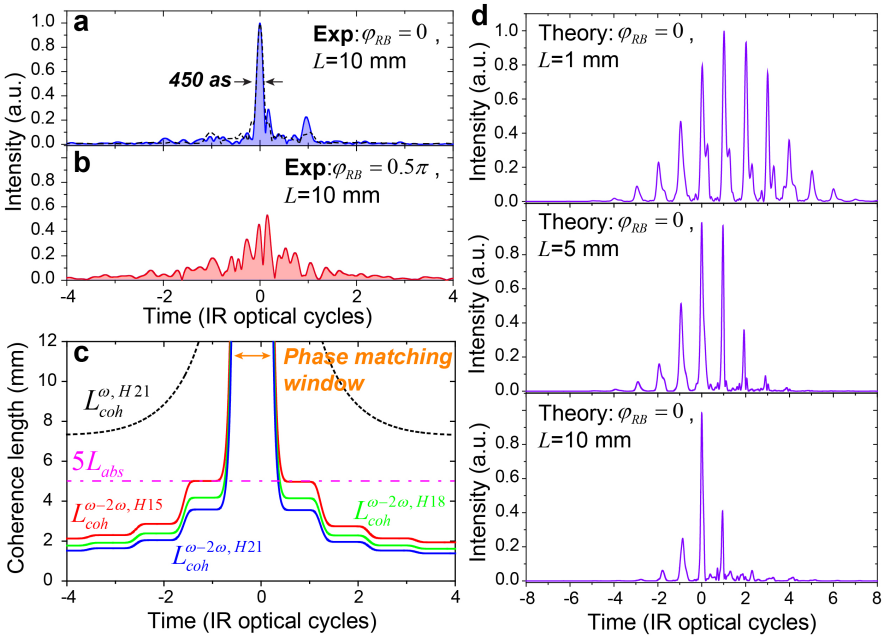

Fig. 3. Quasi-isolated attosecond pulses generated via macroscopic two-color phase-matching gating. a) The quasi-isolated attosecond pulses reconstructed using experimentally measured spectra and phases for $\varphi_{RB} \approx 0$. b) same as (a) for $\varphi_{RB} \approx 0.5\pi$. c) Time-dependent coherence length for a one-color (λ_R=775 nm, dashed line) and two-colors (λ_R=775 nm, λ_B=387.5 nm, solid lines) HHG driven in a 30 torr Ar-filled waveguide. In the one-color case we represent the coherence length of the 21st harmonic (33.6 eV, dashed black), whereas in the two-color case we have selected the 15th harmonic (24 eV, red solid, corresponding to n_R=n_B=5), the 18th harmonic (28.8 eV, green solid, n_R=n_B=6), and the 21st harmonic (33.6 eV, blue solid, n_R=n_B=7). The dot-dashed line represents $5L_{abs}$, where the absorption length is L_{abs} =1 mm for 33.6 eV harmonics [63]. d) The attosecond pulse trains obtained from numerical simulation with two-color driving fields at φ_{RB}=0. The results are calculated by considering the 1D propagation in an Ar-filled waveguide with different interaction length (L= 1 mm, 5 mm and 10 mm). We can clearly distinguish that the number of attosecond bursts decreases as L increases, due to the reduction of phase-matching window, consistent with the analytical representation in (c). When L= 10 mm, only three attosecond pulses are isolated for HHG emission, which is consistent with the experimental results shown in (a).

Optics EXPRESS

particularly at low photon energy where low gas pressure can be used.

4. Controlling the sub-cycle structure of the HHG pulse train

By varying the relative delay between two drivers φ_{RB}, we can control the temporal structure of the emitted HHG pulse train. This is clearly shown by the variation of the pulse train structures (Fig. 3(a) and 3(b)) and the HHG phases (Fig. 2(b)) for different values of φ_{RB}. In Fig. 4a, we plot the evolution of the FWHM duration of attosecond bursts as a function of φ_{RB}, while the results obtained from numerical simulation are shown in Fig. 4b. Due to the complicated pulse train structure in the time domain, especially when $\varphi_{RB} = 0.5\pi$, we calculate the duration of the attosecond bursts (σ) obtained in experiments and simulations in a statistical way by defining the mean-square-weighted deviation (MSWD) within one IR-light cycle (T_R): $\sigma^2 = \frac{\int_0^{T_R} w(t)(t-t_0)^2 \mathrm{d}t}{\int_0^{T_R} w(t)\mathrm{d}t}$, where $w(t)$ is the pulse-train envelope intensity and $t_0 = \frac{\int_0^{T_R} w(t)\times t \mathrm{d}t}{\int_0^{T_R} w(t)\mathrm{d}t}$ is the center-of-mass (COM) of the attosecond pulse. For an ideal Gaussian pulse, σ is the RMS width. In Fig. 4(a), we find that the attosecond burst reaches its shortest FWHM pulse duration ($\Delta t \approx$450 as) when the HHG efficiency is highest at $\varphi_{RB} \approx 0$, while the pulse width gradually increases when the HHG spectral intensity exhibits a minimum at $\varphi_{RB} \approx 0.5\pi$. This result is qualitatively reproduced by our numerical simulations without any free parameters - regardless of the macroscopic propagation distances (Fig. 4(b)) - indicating that it originates from the single-atom response of the two-color driving laser fields.

To understand this dependence of the attosecond pulse duration and the HHG efficiency on the relative delay between the IR and blue laser fields, we implement a semiclassical calculation of electron trajectories. This allows us to extract the ionization and recombination times within the IR optical cycle (pink and green dotted lines, respectively, in Figs. 4(d) and e as well as the corresponding field strength at the moment of ionization and recombination for different φ_{RB}. In the three-step model [23, 24], an atom undergoes tunnel-ionization as the electric field of the laser reaches its maximum value (assuming the process is not saturated). In the quasi-static limit, the ionization rate is given by the ADK model [55], which is proportional to $\exp(-\frac{4\sqrt{2m_e E_a^3}}{3e\hbar|E_{\mathrm{ion}}|})$, where E_a=15.8 eV is the ionization potential of argon, E_{ion} is the field strength at the moment of ionization, and m_e and e are the mass and charge of an electron, respectively. The value of E_{ion} depends on φ_{RB} and reaches the maximum value when $\varphi_{RB} = 0.0$, as shown in Fig. 4(c). At the same time, the HHG efficiency reduces with the increase of the excursion time of ionized electrons with longer trajectories, due to the dispersion of the wave packet [64, 65]. Comparing the excursion times ($\tau_m^{\mathrm{emit}} - \tau_m^{\mathrm{ion}}$ with m =1, 2, 3), we find the excursion times for φ_{RB}=0.5π (m =2, 3) is longer than that of φ_{RB}=0.0 (m =1). This further contributes to the reduction of HHG efficiency when φ_{RB}=0.5π. Therefore, within the three-step model of HHG, the efficiency of harmonic emission under the two-color driving configuration is controlled by the total ionization rate, as well as the dispersion of the electron wavefunction during the excursion times.

On the other hand, the ionization and recombination steps are influenced by the symmetry of the two-color driving field in the time domain. As shown in Fig. 4(c), when $\varphi_{RB} = 0$, the laser field exhibits a single maximum in each IR optical cycle (τ_1^{ion}). The field strength at the second maximum is much lower (60% of the peak field strength) so that the corresponding electron ionization probability is negligible. As a result, the attosecond EUV burst is only emitted in the corresponding narrow recombination window around τ_1^{emit}, as shown by the time-frequency analysis [66] (see Fig. 4(d)), leading to the shortest HHG pulse duration. In contrast, when φ_{RB} = 0.5π, there exist two maxima with comparable field strength within each IR optical cycle (τ_2^{ion} and τ_3^{ion}), as shown in Fig. 4(c). Both maxima can induce ionization and subsequent recombination events (τ_2^{emit} and τ_3^{emit}), which gives rise to the HHG emission shown in Fig. 4(e), leading to

Optics EXPRESS

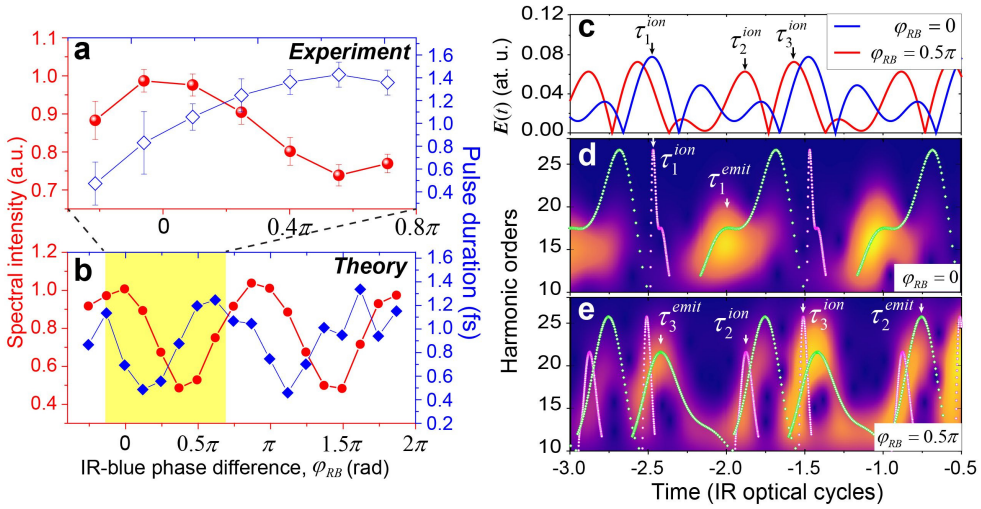

Fig. 4. Controlling attosecond fields using two-color driving lasers. a) Experimentally measured HHG intensity and FWHM pulse width of the attosecond bursts as a function of φ_{RB}. b) Same as (a) obtained from the numerical simulation. The yellow-colored section highlights the range of φ_{RB} probed in our experiments as shown in (a). c) The time-dependent electric field contributed by the combined two-color driving fields with relative phase between two fields at $\varphi_{RB} = 0$ and $\varphi_{RB} = 0.5\pi$. d) Time-frequency analysis for the pulse train generated at $\varphi_{RB} = 0$ obtained from the numerical simulation. The electron ionization (magenta open circles) and recombination times (green open diamonds) are plotted and overlaid on the figure. Clearly, at $\varphi_{RB} = 0$ electrons recombine and harmonics are efficiently generated only in a single time window (τ_1^{emit}) within every IR optical cycle, corresponding to a single ionization time τ_1^{ion} (also see (c)). e) Same as the (d) for $\varphi_{RB} = 0.5\pi$. Different from the situation when $\varphi_{RB} = 0$, the two-color fields drive electrons to recombine and emit HHG photons in two time windows (τ_2^{emit} and τ_3^{emit}) every IR optical cycle, which corresponds to ionization times τ_2^{ion} and τ_3^{ion}, respectively. This additional ionization and recombination time window leads to additional attosecond temporal structure in the HHG pulse trains driven by two-color laser field as shown in Fig. 3(b).

additional attosecond EUV bursts in the time domain (Fig. 3(b)).

5. Conclusion

In summary, we investigated attosecond waveforms driven by a two-color linearly polarized laser field. Characterization of the HHG phases using interferometric laser-assisted photoelectron spectroscopy revealed several new findings. First, we observe that the temporal window for efficient harmonic emission is significantly reduced for a two-color driving field compared to a one-color laser, shrinking to 450 as in duration using long (26 fs) driver pulses. A comparison between our experimental data and numerical simulations confirmed that this effect is due to enhanced macroscopic phase-matching gating in a two-color driving field, which decreases by a factor of 4 compared to a one-color driving laser field. Finally, we demonstrated that the temporal structure of the attosecond pulse trains can be controlled by adjusting the delay between the two laser fields. These results show that two-color phase matching gating is a powerful tool for tailoring attosecond waveforms, that does not require mid-infrared driving laser pulses.

Optics EXPRESS

Funding

National Science Foundation (NSF) (1125844); Air Force Office of Scientific Research (FA9550-16-1-0121); REA (328334); Junta de Castilla y León (SA046U16); MINECO (FIS2013-44174-P, FIS2016-75652-P).

Acknowledgments

We thank A. Carr, P. Matyba, R. Knut, P. Gychtol and E. Turgut for helpful discussions. M.M., H.K., A.B. and A. J-B. gratefully acknowledge support from the NSF through the PFC Program Award No. PHY 1125844 (experiment) as well as a MURI grant from the AFOSR under Award No. FA9550-16-1-0121 (theory). C.H.-G. acknowledges support from the Marie Curie IOF within the EU Seventh Framework Programme for Research and Technological Development (2007-2013), under REA grant Agreement No. 328334, from Junta de Castilla y León (SA046U16) and from MINECO (FIS2013-44174-P, FIS2016-75652-P). Disclosure: The authors declare that they have no competing interests. H.K. and M. M. are partial owners of a laser company, KMLabs.